



Icariin alleviates uveitis by targeting peroxiredoxin 3 to modulate retinal microglia M1/M2 phenotypic polarization

Guoqing Wang^{a,b,c,d,1}, Xingran Li^{a,b,c,d,1}, Na Li^e, Xiaotang Wang^{a,b,c,d}, Siyuan He^{a,b,c,d},
Wanqian Li^{a,b,c,d}, Wei Fan^{a,b,c,d}, Ruonan Li^{a,b,c,d}, Jiangyi Liu^{a,b,c,d}, Shengping Hou^{a,b,c,d,*}

^a The First Affiliated Hospital of Chongqing Medical University, Chongqing, China

^b Chongqing Key Laboratory of Ophthalmology, Chongqing, China

^c Chongqing Eye Institute, Chongqing, China

^d Chongqing Branch of National Clinical Research Center for Ocular Diseases, Chongqing, China

^e College of Basic Medicine, Chongqing Medical University, Chongqing, 400016, China

ARTICLE INFO

Keywords:

Icariin
Uveitis
PRDX3
Microglia
M1 phenotype
M2 phenotype

ABSTRACT

Uveitis causes blindness and critical visual impairment in people of all ages, and retinal microglia participate in uveitis progression. Unfortunately, effective treatment is deficient. Icariin (ICA) is a bioactive monomer derived from Epimedium. However, the role of ICA in uveitis remains elusive. Our study indicated that ICA alleviated intraocular inflammation *in vivo*. Further results showed the proinflammatory M1 microglia could be transferred to anti-inflammatory M2 microglia by ICA in the retina and HMC3 cells. However, the direct pharmacological target of ICA is unknown, to this end, proteome microarrays and molecular simulations were used to identify the molecular targets of ICA. Data showed that ICA binds to peroxiredoxin-3 (PRDX3), increasing PRDX3 protein expression in both a time- and a concentration-dependent manner and promoting the subsequent elimination of H₂O₂. In addition, GPX4/SLC7A11/ACSL4 pathways were activated accompanied by PRDX3 activation. Functional tests demonstrated that ICA-derived protection is afforded through targeting PRDX3. First, ICA-shifted microglial M1/M2 phenotypic polarization was no longer detected by blocking PRDX3 both *in vivo* and *in vitro*. Next, ICA-activated GPX4/SLC7A11/ACSL4 pathways and downregulated H₂O₂ production were also reversed via inhibiting PRDX3 both *in vivo* and *in vitro*. Finally, ICA-elicited positive effects on intraocular inflammation were eliminated in PRDX3-deficient retina from experimental autoimmune uveitis (EAU) mice. Taking together, ICA-derived PRDX3 activation has therapeutic potential for uveitis, which might be associated with modulating microglial M1/M2 phenotypic polarization.

1. Introduction

Autoimmune uveitis (AU), characterized by immune-mediated chronic inflammatory intraocular disorders, is one of the main causes of visual impairment and blindness [1,2]. A robust model of human uveitis is experimental autoimmune uveitis (EAU), which can be induced by immunization with interphotoreceptor retinoid-binding protein (IRBP) [3]. Although immunosuppressive treatments including corticosteroids, antimetabolites, and alkylating agents are effective therapies, the nonspecific nature and the side effects preclude their long-term application [4]. Thus, searching more effective and less side-action therapeutic potential treatments is urgent.

Although the etiology of uveitis remains largely unknown, strong evidence has shown that uveitis is associated with oxidative stress [5,6]. Accumulated reactive oxygen species (ROS) including hydrogen peroxide (H₂O₂) can disrupt retinal homeostasis. H₂O₂ is usually produced in mitochondria and can activate mitochondrial oxidative damage [7]. Peroxiredoxins (PRDXs), including at least 6 isoforms, are a family of thiol peroxidases. Among them, PRDX3 is the main species in mitochondria [8]. As an important mitochondrial antioxidant protein, PRDX3 is the most plentiful and efficient H₂O₂ eliminating enzyme in mitochondria, playing a major role against oxidative stress [9]. Being oxidized into inactive dimer form, PRDX3 scavenges H₂O₂ and effectively prevents oxidative stress, apoptosis and cellular damage [10]. The

* Corresponding author. The First Affiliated Hospital of Chongqing Medical University, Chongqing, 400016, China.

E-mail address: sphou828@163.com (S. Hou).

¹ These authors contributed equally.

<https://doi.org/10.1016/j.redox.2022.102297>

Received 23 February 2022; Received in revised form 10 March 2022; Accepted 16 March 2022

Available online 18 March 2022

2213-2317/© 2022 Published by Elsevier B.V. This is an open access article under the CC BY-NC-ND license (<http://creativecommons.org/licenses/by-nc-nd/4.0/>).

increase of mitochondrial H₂O₂ is a critical pathological process of EAU. Increased PRDX3 expression in some neurons may represent a basic protective mechanism that can reduce oxidative stress injury [11]. Hence, reducing the overproduction of H₂O₂ via PRDX3 may ameliorate retinal damage during EAU.

Meanwhile, microglia-elicited inflammatory processes also participate in the progression of uveitis [12]. Microglia are resident immune cells of the retina, and activated microglia release inflammatory factors including tumor necrosis factor (TNF- α) cyclooxygenase-2 (COX-2), inducible nitric oxide synthase (iNOS), which further aggravate retinal damage and blood–retina barrier (BRB) dysfunction. In turn, overproduction of inflammatory factors further results in microglial reactivation, and reactivated microglia release more inflammatory factors, frequently aggravating the uncontrolled inflammatory cascade in the retina [13,14]. Microglia activation states can be divided into a proinflammatory M1 state and an anti-inflammatory M2 state. LPS is an agonist of M1 microglia, COX-2, iNOS, TNF- α and nitric oxide (NO) are markers of M1 microglia. In contrast, arginase 1 (ARG1), CD206 and interleukin 10 (IL-10) are markers of M2 microglia that not only inhibit the expression of proinflammatory mediators but also facilitate neuroprotection [15,16]. Thus, promoting the transformation of microglia from the M1 state to the M2 state may ameliorate retinal damage in EAU.

Icariin (ICA), a flavone compound extracted from *Epicedium*, shows a range of pharmacological functions, such as anti-oxidation, anti-inflammation and anti-aging effects both in vivo and in vitro, as multiple studies have concluded [17]. ICA has also been reported to inhibit LPS-induced inflammation in mouse peritoneal macrophages and peritonitis models [18]. Furthermore, ICA could reduce inflammatory penetration in neurological disorder models by passing the blood-brain barrier [19]. In addition, ICA protected dopamine neuronal damage against LPS-induced neurotoxicity in the Parkinson's disease animal model [20]. Although the neuroprotective effects of ICA in the CNS system are well documented, the role and mechanism of ICA in EAU are poorly understood.

This study was conducted to explore the protective effects of ICA in the progression of EAU and to understand its underlying mechanisms. We utilized IRBP-induced EAU mice and LPS-induced inflammatory HMC3 cells in this study, we reported that ICA alleviated intraocular inflammation in vivo and shifted the microglial M1/M2 phenotypic polarization in the retina and HMC3 cells. Further studies revealed that ICA alleviated EAU by directly acting on microglia in a PRDX3-dependent manner. We revealed the critical role of ICA in EAU retina one of which is to maintain M1/M2 phenotype homeostasis and the other of which is to protect the retina from H₂O₂-mediated damage by increasing PRDX3.

2. Material and methods

2.1. Reagents

Icariin (HPLC identified purity as 98.04%) was purchased from Topscience (Shanghai, China). Human IRBP₆₅₁₋₆₇₀ (LAQGAYRTAV-DLESLASQLT) (purity >98%) was synthesized by Sangon Bioengineering Technology and Services Co., Ltd. (Shanghai, China). Lipopolysaccharide (O111:B4) and complete Freund's adjuvant were obtained from Sigma-Aldrich (St. Louis, Missouri, USA). Heat-killed *M. tuberculosis* strain H37Ra was got from BD Biosciences (New Jersey, USA). Pertussis toxin (PTX) was obtained from Sigma-Aldrich (St. Louis, Missouri, USA).

2.2. Animals

Female C57BL/6J mice (6–8 weeks) were purchased from The Experimental Animal Center of Chongqing Medical University. All animal experiments strictly abided by the management of the Ethics Committee of the First Affiliated Hospital of Chongqing Medical

University. All the animals were kept in a specific pathogen free facility under constant temperature and relative humidity conditions.

2.3. EAU induction and ICA treatment

Human IRBP₆₅₁₋₆₇₀ (500 mg) was dissolved in PBS (1 ml) and *M. tuberculosis* strain H37Ra (40 mg) was dissolved in Freund's adjuvant (1 ml). Next, IRBP and Freund's adjuvant were emulsified with an equal volume (1:1, v/v) for 1 h. Mice received subcutaneous injection of IRBP (500 μ g) and intraperitoneal injection of PTX (1 μ g) for EAU model [21]. After EAU induction for 7 days, all immunized mice were examined with slit lamp to guarantee model success. All mice were randomly divided into three groups according to the different treatments: the Control group and the EAU group received intragastric administration of saline; the EAU + ICA group received intragastric administration of ICA (10 mg/kg/day) for 7 consecutive days. Next, the clinical severity of ocular inflammation was examined by slit lamp according to five independent criteria and Caspi's criteria. Then, the mice were sacrificed for the following experiments.

2.4. Integrity of the blood-retinal barrier (BRB)

Evans Blue dye (2%, 100 μ L, Sigma-Aldrich) was injected through the tail vein. After blood circulation for 2 h, eyeballs were obtained and submerged in 4% paraformaldehyde for 2 h. The retina was carefully stripped and made into a four-leaf clover shape. BRB integrity was observed by microscope (Leica, Germany).

2.5. Immunofluorescence staining

According to the abovementioned methods, the retinal four-leaf clover shape was permeabilized with 3% Triton X-100 for 15 min and blocked with bovine serum albumin for 2 h. Next, the retina was incubated with IBA1 antibody (1:500, Abcam, USA) at 4 °C overnight. After washing, the retina was incubated with Alexa-488 (green) conjugated goat anti-rabbit IgG (1:3000, Abcam, USA) for 1 h. Images were taken under the microscope (Leica, Germany).

2.6. Hematoxylin and eosin (H&E) staining

The eyeballs were embedded in paraffin wax and sectioned to 4–6 μ m thickness. After dewaxing with xylene, the slides were dehydrated in absolute ethanol, 95% alcohol, 85% alcohol and 75% alcohol for gradient dehydration for 5 min/each time. Antigens were repaired in citrate antigen repair buffer (pH 6.0) (Servicebio, Wuhan, China). Sections were stained with H&E and each eye was scored based on Caspi's criteria.

2.7. Proteome microarray assays

The HuProt microarray was obtained from the Johns Hopkins Medical Institutions Protein Microarray Core (CDI Laboratories, Inc). The array experiment was performed by Wayen Biotechnologies (Shanghai, China) according to the following procedure. Briefly, the proteome microarrays were immersed in blocking buffer and incubated with biotin (10 μ M) and Biotin-icariin (10 μ M) for 1 h. After washing, proteome microarrays were put into 0.1% Cy5-Streptavidin solution for 20 min in the dark. After washing and centrifuging (1000 \times g, 2 min), the microarrays were scanned with a GenePix 4000B microarray scanner (Axon Instruments, CA).

2.8. Network analyses

The Search Tool for Recurring Instances of Neighboring Genes (STRING) system, a database of protein-protein interactions, was used to build the biological interaction networks for PRDX3. The organism and

confidence were set to “*Homo sapiens*”, “20 connections” and “high-confidence”, respectively.

2.9. Molecular docking of ICA to PRDX3

The crystal structure of PRDX3 was derived from Protein Data Bank and the 3D structure of ICA was obtained from PubChem. Before testing, the structures of PRDX3 and ICA were ensured to be in the optimized active arrangement. Finally, the Glide SP (standard precision) scoring function was used for docking.

2.10. HMC3 cell line

The human microglial cell line (HMC3) was obtained from the American Type Culture Collection (ATCC). Briefly, cells were maintained in eagle's minimum essential medium (EMEM) supplemented with 10% FBS, 50 U/ml penicillin, and 50 µg/ml streptomycin in a humidified incubator. The cells were seeded in 6-well plates at 5×10^5 cells/well for 24 h, and HMC3 cells were randomly divided into Control, LPS (1 µg/ml) + IFN- γ (500 ng/ml) and LPS (1 µg/ml) + IFN- γ (500 ng/ml) + ICA (10 µM) groups. Another 24 h later, cells and supernatant were collected.

2.11. Cell viability

Cells were seeded in 96-well plates at a density of 8000 cells/100 µL for 24 h. Following ICA and Biotin-ICA (0.01, 0.05, 0.1, 0.5, 1, 5, 10, 20 µM) treatments for 24 h, CCK8 solutions were added and HMC3 cells were incubated at 37 °C for 1.5 h. Then, the absorbances were detected at 450 nm.

2.12. TNF- α , COX-2, nitric oxide (NO) assays

Griess reagent was used to quantify the production of NO by measuring increased levels of nitrite in the supernatant. The production of TNF- α and COX-2 in the supernatant were measured by ELISA kits from R&D Systems following the manufacture's protocol.

2.13. Quantitative real-time PCR

RT Master Mix for qPCR (Cat.No. HY-K0510; Lot No.80770) and SYBR Green qPCR Master Mix (Cat.No. HY-K0522; Lot No.107813) were purchased from Med Chem Express (Shanghai, China). Total RNA of cells or tissues was isolated using TRIzol reagent. The mRNA levels were assessed using RT Master Mix and SYBR Green qPCR Master Mix based on the manufacturer's recommended protocol. RNA levels were normalized to GAPDH. All primers of targeted genes have been shown in Table S1.

2.14. Western blot assays

Ten-percent Bis-Tris-polyacrylamide electrophoresis gels were used to separate equal amounts of proteins, and proteins were transferred to PVDF membranes. Following blocking with 5% nonfat milk, the membranes were incubated with primary antibody overnight at 4 °C. The following antibodies were purchased from Proteintech: TNF- α (1:1000, Cat.No. 17590-1-AP), COX-2 (1:1000, Cat.No. 12375-1-AP), iNOS (1:1000, Cat.No. 18985-1-AP), ARG1 (1:1000, Cat.No. 16001-1-AP), CD206 (1:1000, Cat.No. 18704-1-AP), PRDX3 (1:2000, Cat.No. 10664-1-AP), SLC7A11 (1:1000, Cat.No. 26864-1-AP), goat anti-rabbit IgG (1:5000, Cat.No. SA00001-2), goat anti-mouse IgG (1:5000, Cat.No. SA00001-1). IL-10 (1:500, ab189392), IBA1 (1:1000, ab178846), β -actin (1:2000, ab8226) and occludin (1:500, ab222691) were purchased from Abcam. GPX4 (1:1000, sc-166570) and ACSL4 (1:1000, sc-365230) were obtained from Santa Cruz Biotechnology. The membranes were incubated with anti-rabbit or mouse IgG for 1 h and detected by

ECL Plus reagents. The amounts of proteins were analysed using ImageJ and normalized to the amount of β -actin.

2.15. Retina and HMC3 H₂O₂ measurements

Hydrogen peroxide assay kit (Nanjing Jiancheng Corp., China) was applied to quantify the H₂O₂ levels of the retina and HMC3 cells based on the manufacturer's recommended protocol. A firmness complex was formed after the reaction with H₂O₂, and its absorbance was measured at 405 nm.

2.16. Cell transfection for silencing

The PRDX3-shRNA and Vehicle-shRNA were purchased from GeneChem (Shanghai, China). HMC3 cells were transfected with PRDX3-shRNA (MOI = 10) or Vehicle-shRNA (MOI = 10) for 10 h. After changing the medium, HMC3 cells were cultured with puromycin (2 µg/ml)-containing medium. Transfective cells were seeded in 6-well plates at 5×10^5 cells/well. Twenty-four hours later, cells were received LPS (1 µg/ml) + IFN- γ (500 ng/ml) + ICA (10 µM) administration. Another 24 h later, cells and supernatant were collected to measure the specific indicator.

2.17. Statistical analysis

All the data were presented as the means \pm SDs and analysed by SPSS 20.0 software. Unpaired Student's *t*-test was applied to assess significance between two groups. One-way ANOVA was applied to multiple groups, which was corrected by Least Significant Difference (LSD) analysis. For clinical scores and pathological scores, Kruskal-Wallis test was applied to multiple groups and Mann-Whitney *U* test was applied to two groups. The differences at $p < 0.05$ were considered to be statistically significant.

3. Results

3.1. ICA alleviated EAU progression in vivo

To investigate whether ICA could alleviate intraocular inflammation, EAU mice received intragastric treatment with ICA (10 mg/kg/day) for 7 consecutive days. Next, the clinical symptoms and histopathological staining were examined. As shown in Fig. 1B, ICA significantly decreased the conjunctival and ciliary hyperaemia as well as infiltration of anterior chamber inflammatory cells (Fig. 1B). As indicated in Fig. 1C, H&E staining revealed fewer retinal folds and inflammatory cells in the EAU + ICA group (Fig. 1C). This clinical score and pathological score results were consistent with the abovementioned phenomenon. In addition, to examine the effect of ICA on BRB breakdown, we measured the integrity of BRB. The results indicated that ICA significantly relieved leakage accompanied by increased occludin expression (Fig. 1D). Furthermore, to detect the influence of ICA on microglia, morphological changes as well as microglial activation were investigated by immunostaining for a specific microglial marker (IBA1). As illustrated in Fig. 1E, there were many activated microglia in the EAU group, which was characterized by strengthened IBA1 staining and expanded rounded cell size. Interestingly, microglia in ICA-treated mice displayed normal morphology and a similar level of IBA1 expression compared to those in the Control group, suggesting that microglial activation is blocked by ICA (Fig. 1E).

3.2. ICA promoted the phenotypic polarization of M1 microglia to M2 microglia in vivo and in vitro

The results shown in Fig. 1E prompted us to explore whether ICA could promote microglial M1/M2 phenotypic polarization. We used retina and HMC3 cells to determine the levels of M1 microglial markers

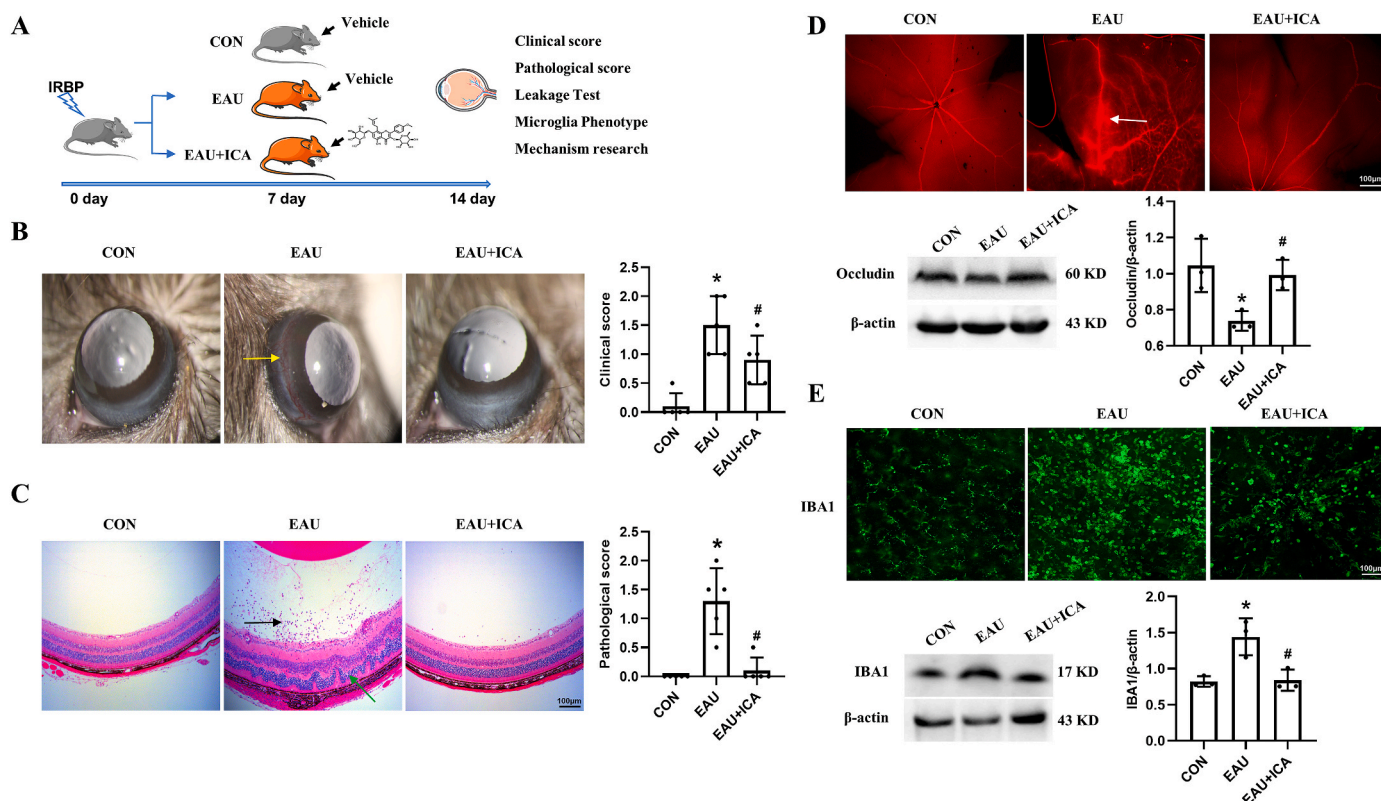


Fig. 1. ICA alleviated EAU progression in vivo (A) The schematic of animal experimental design. (B–C) Anterior chamber inflammation and retinal histopathological staining in the Control, EAU and EAU + ICA groups. Clinical scores and pathology scores were also exhibited. (scale bar, 100 μ m; yellow arrows, conjunctival and/or ciliary congestion; black arrow, infiltration of inflammatory cells; green arrow, retinal folds). (D) Retinal integrity in the Control, EAU and EAU + ICA groups. Retinal ocludin quantification was detected by Western blotting (scale bar, 100 μ m, white arrow, retinal vascular leakage). (E) Retinal microglia staining in the Control, EAU and EAU + ICA groups. Further quantification of retinal IBA1 was performed by Western blotting (scale bar, 100 μ m). * p < 0.05 compared with the Control group; # p < 0.05 compared with the EAU group. (n = 3–5).

(TNF- α , COX-2, iNOS) and M2 microglial markers (ARG1, CD206 and IL-10). As shown in Fig. 2, the EAU group exhibited elevated protein expression of M1 markers and reduced protein levels of M2 markers. As expected, ICA treatment reversed EAU-elicited microglial phenotypic polarization (Fig. 2A and B). Next, HMC3 cells were randomly divided into Control group, LPS (1 μ g) + IFN- γ (500 ng) group and LPS (1 μ g) + IFN- γ (500 ng) + ICA (10 μ M) group. Twenty-four hours later, cells and supernatant were collected to measure M1/M2 phenotypic polarization. As indicated in Fig. 2, LPS + IFN- γ addition markedly increased the protein levels of M1 markers and declined the protein expression of M2 markers, which was greatly reversed by ICA (10 μ M) treatment (Fig. 2C and D). These data, combined with Fig. 1E implied that ICA could change M1 microglia to M2 microglia.

3.3. Identification of ICA-binding proteins

We utilized HuProt microarray, which consisted of 20,000 affinity-purified GST-tagged proteins to screen for ICA-binding proteins [22]. Briefly, we incubated biotin-labelled ICA (Biotin-ICA) or biotin with the HuProt microarray, and used Cy5-coupled streptavidin (Cy5-SA) to identify proteins with ICA-binding capacity (Fig. 3A). The molecular structure of ICA and Biotin-ICA were shown in Fig. 3B. Next, CCK8 assay indicated that at the experimental concentration, both ICA and Biotin-ICA had no effect on cell viability (Fig. 3C). A partially enlarged view of biotin and Biotin-ICA proteome microarrays were shown in Fig. 3D. In venn diagram, after nonspecific signals were removed, 246 proteins were identified as ICA-binding candidate proteins. The IMean ratio of two repeated spots was evaluated to standardize the data, which was set to ≥ 1.414 . In descending order of IMean ratio, 22 proteins were

selected (Fig. 3E). Then, Gene Ontology (GO) analysis was applied to examine the 246 candidate proteins (Fig. 3F). Furthermore, to understand the functional roles of ICA-binding proteins deeply, the 246 proteins were used for KEGG pathway enrichment. A substantial enrichment in metabolic pathways, glutathione metabolism and purine metabolism were found in the KEGG pathway (Fig. 3G).

3.4. PRDX3 is a target of ICA

Among the selected 22 proteins, the highest-ranking protein was ALDH9A1 (IMean ratio of 2.301), and the second was PRDX3 (IMean ratio of 2.095). ALDH9A1 belongs to the aldehyde dehydrogenase family of proteins [23]. However, we did not observe any changes in the Control, EAU or EAU + ICA group (Fig. S1). PRDX3 encodes a mitochondrial protein with antioxidant function [9]. Research has shown that oxidative stress plays a vital role in the progression of uveitis [5]. Thus, we selected PRDX3 for functional verification. Enlarged images of PRDX3 in the proteome microarray were shown in Fig. 4A. Further molecular docking showed that ICA may bind to PRDX3 in the pocket between the two chains. Hydroxyl groups on the ICA form hydrogen bonds with Lys135 and Glu162 on chain A and Thr44 on chain B (Fig. 4B). Furthermore, we detected the presence of retinal PRDX3 protein, as shown in Fig. 4C, PRDX3 exhibited higher expression in the EAU + ICA group than in the EAU group (Fig. 4C). To verify the effect of ICA on PRDX3 in microglia, HMC3 cells were pretreated with ICA (0.1 μ M, 1 μ M and 10 μ M) and then stimulated with LPS + IFN- γ for 24 h. The results indicated that ICA (0.1 μ M–1 μ M) showed no effect on PRDX3 protein expression, while there was a significant increase in PRDX3 with ICA (10 μ M) (Fig. 4D). Furthermore, HMC3 cells were

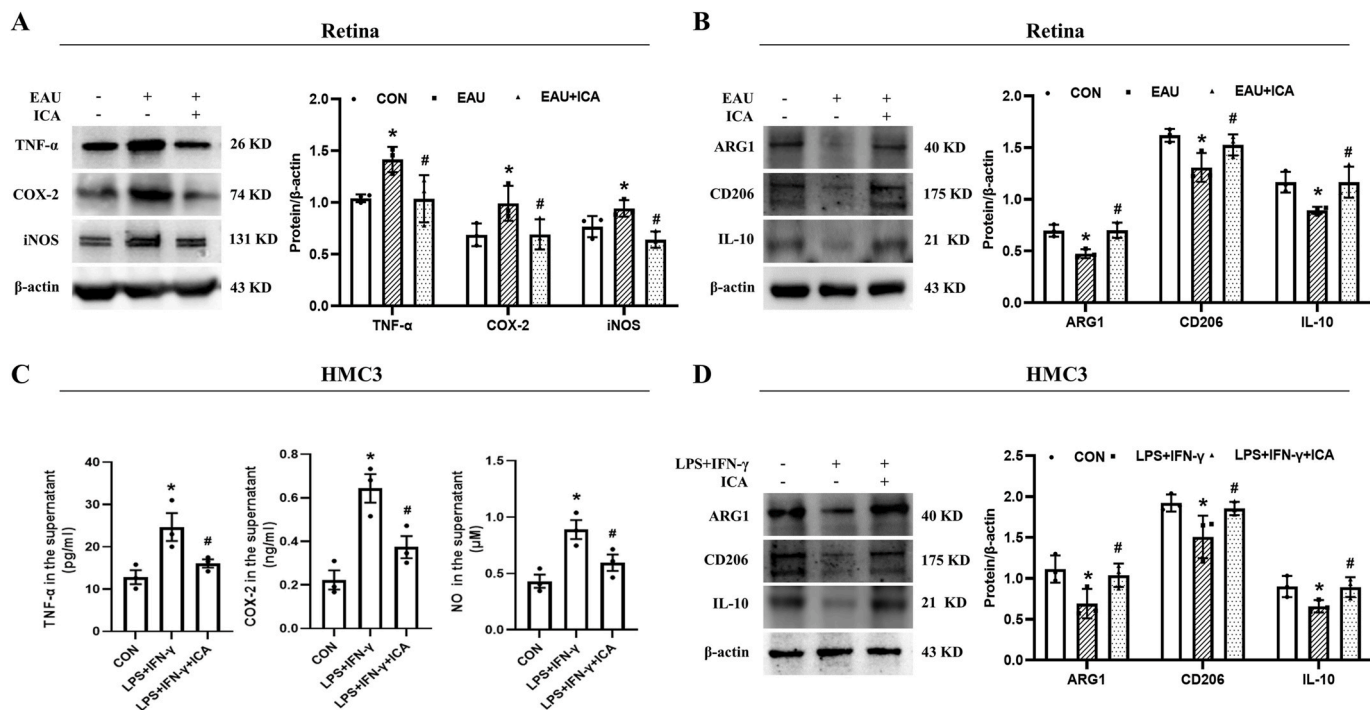


Fig. 2. ICA promoted the phenotypic polarization of M1 microglia to M2 microglia in vivo and in vitro (A-B) Retinal microglial M1 markers (TNF- α , COX-2, iNOS) and M2 markers (ARG1, CD206, IL-10) in the Control, EAU and EAU + ICA groups were measured by Western blotting, respectively. (C) HMC3 cells M1 markers (TNF- α , COX-2, NO) in the Control, LPS + IFN- γ and LPS + IFN- γ + ICA groups were revealed by ELISA. (D) HMC3 cells M2 markers (ARG1, CD206, IL-10) in the Control, LPS + IFN- γ and LPS + IFN- γ + ICA groups were measured by Western blotting. * p < 0.05 compared with the Control group; # p < 0.05 compared with the EAU group or LPS + IFN- γ group. (n = 3).

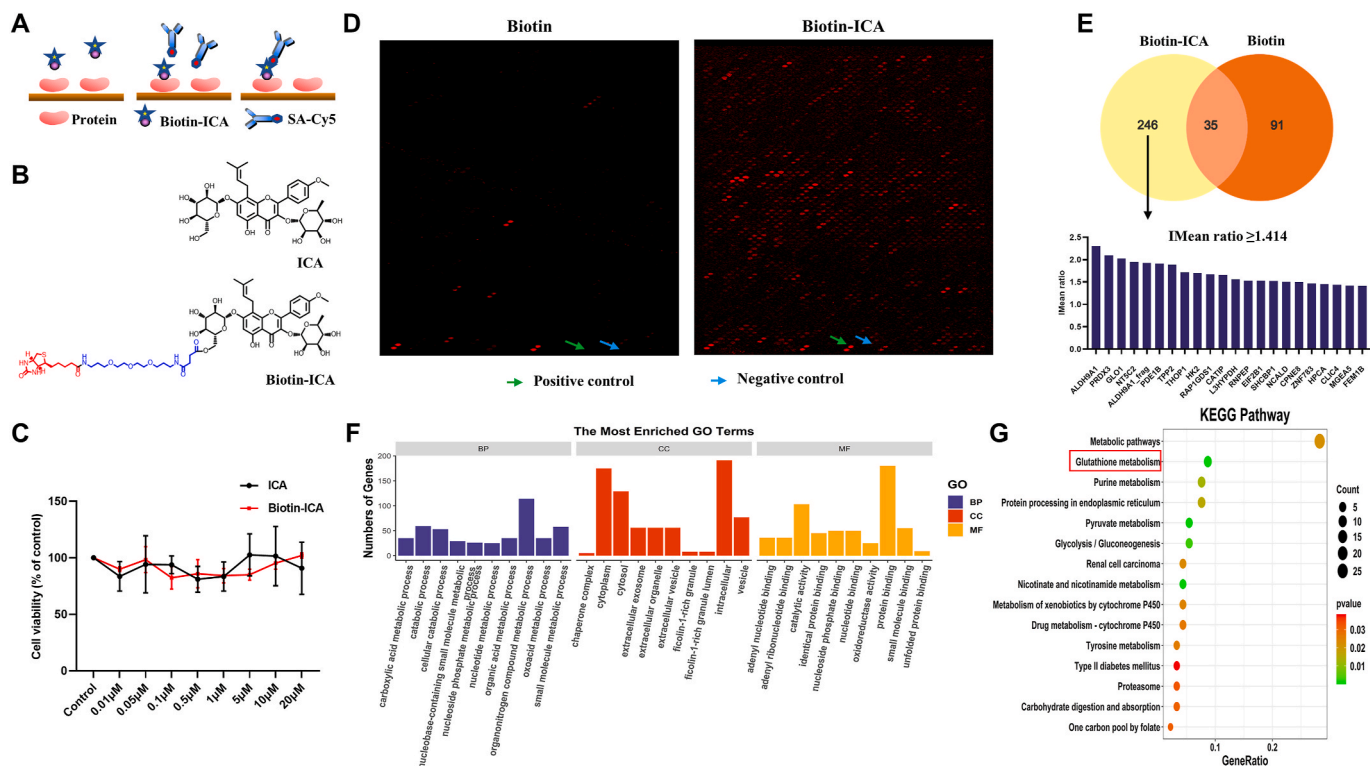


Fig. 3. Identification of ICA-binding proteins on human proteome microarrays (A) Schematic of the procedure for detecting ICA-binding proteins using human proteome microarrays. (B) Molecular structure of ICA and biotin-labelled (red) ICA (Biotin-ICA). (C) CCK8 assays were used to detect the HMC3 viability treated with ICA and Biotin-ICA. (D) Human proteome microarrays were probed with Biotin (left) and Biotin-ICA (right). Representative images of protein array showed positive spots (green arrow) and negative spots (blue arrow) on the partial area of microarrays. (E) Venn diagram for Biotin-ICA target proteins and biotin target proteins. Yellow arrow represents the number of ICA specific target proteins. In descending order of IMean ratio, 22 proteins were selected. (F) GO analysis of ICA-binding proteins. (G) KEGG pathway of ICA-binding proteins.

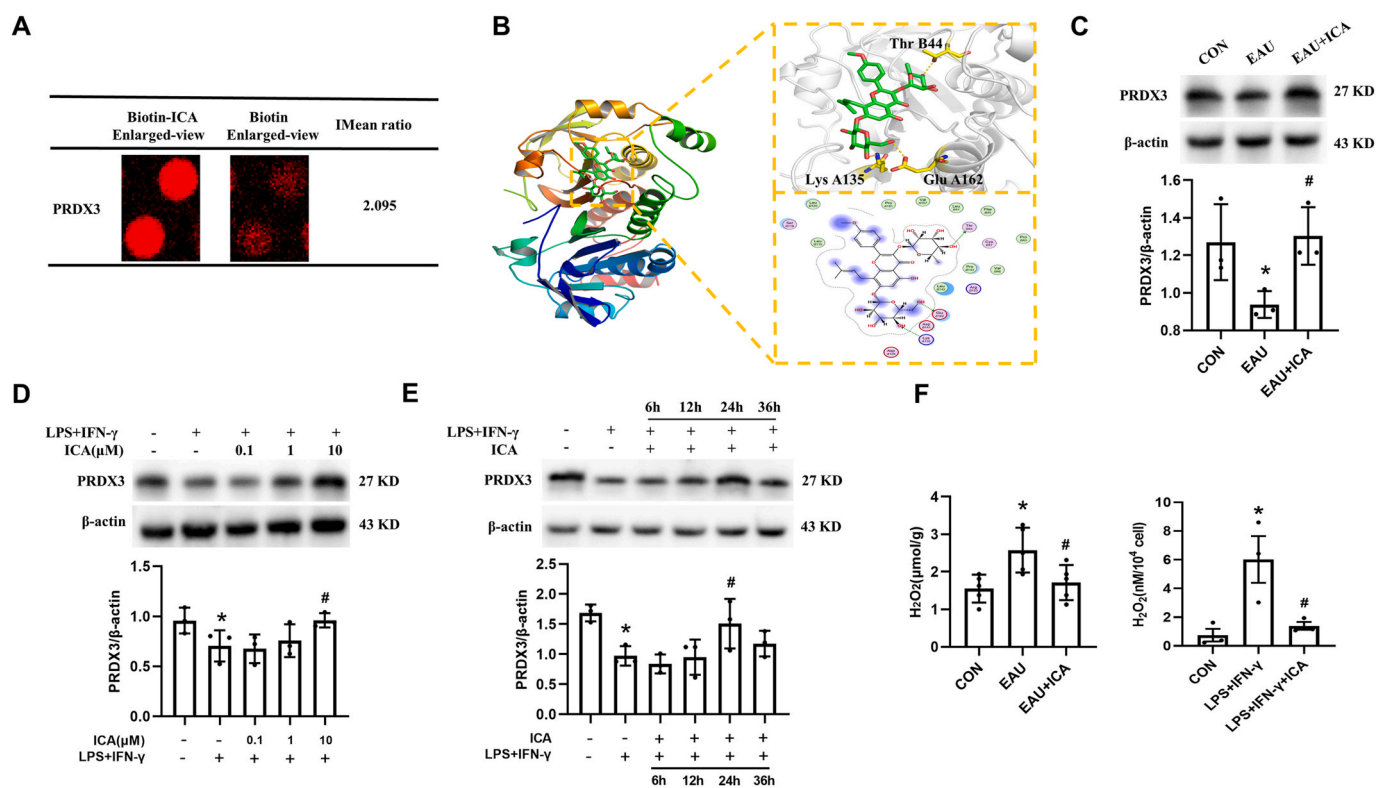


Fig. 4. PRDX3 is a target of ICA (A) Enlarged images of PRDX3 of the proteome microarray results. (B) ICA may bind to PRDX3 in the pocket between the two chains. Hydroxyl groups on ICA form hydrogen bonds with Lys135 and Glu162 on chain A and Thr44 on chain B. (C) Retinal PRDX3 protein levels in the Control, EAU and EAU + ICA groups as revealed by Western blotting. (D) HMC3 cells were pretreated with ICA (0.1 μM, 1 μM and 10 μM) for 1 h and then stimulated with LPS + IFN-γ for 24 h. PRDX3 protein levels were measured by Western blotting. (E) HMC3 cells were pretreated with ICA (10 μM) for 1 h and then stimulated with LPS + IFN-γ for 6 h, 12 h, 24 h and 36 h. PRDX3 protein levels were measured by Western blotting. (F) H₂O₂ level were measured in vivo and in vitro. **p* < 0.05 compared with the Control group; #*p* < 0.05 compared with the EAU/LPS + IFN-γ group. (n = 3-5).

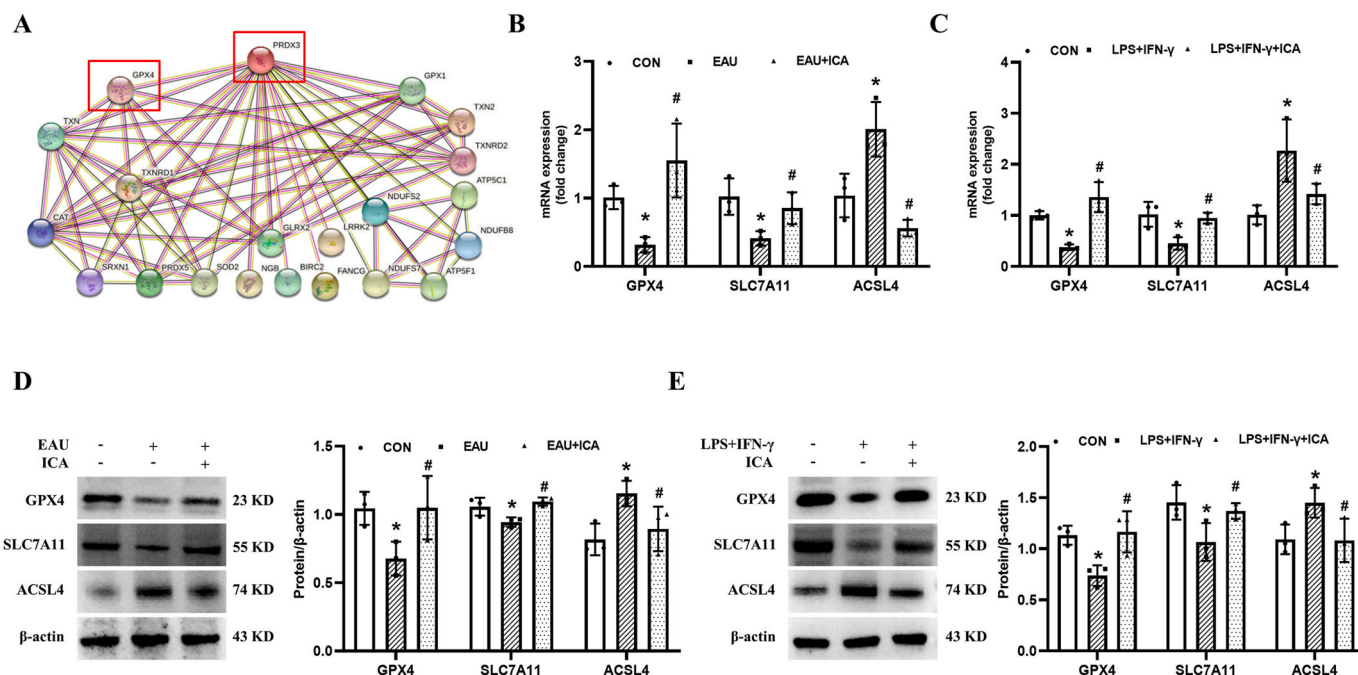


Fig. 5. ICA regulated the GPX4/SLC7A11/ACSL4 pathways (A) Biological interaction networks of PRDX3 for the top 20 connections according to the STRING system with the “*Homo sapiens*” and “high-confidence” settings. (B and D) Retinal GPX4, SLC7A11 and ACSL4 mRNAs and protein expression in the Control, EAU and EAU + ICA groups were measured respectively. (C and E) Microglial GPX4, SLC7A11 and ACSL4 mRNAs and protein expression in the Control, LPS + IFN-γ and LPS + IFN-γ + ICA groups were revealed respectively. **p* < 0.05 compared with the Control group; #*p* < 0.05 compared with the EAU/LPS + IFN-γ group. (n = 3).

pretreated with ICA (10 μ M) for 1 h and then stimulated with LPS + IFN- γ for 6 h, 12 h, 24 h and 36 h. As shown in Fig. 4E, PRDX3 expression increased only after ICA (10 μ M) treatment for 24 h (Fig. 4E). The in vitro results suggested that ICA increased PRDX3 protein expression in time- and concentration-dependent manner. In addition, PRDX3 is a H₂O₂ scavenger, whether ICA-elicited higher PRDX3 accompanied by enhanced H₂O₂ clearance is unclear. Thus, we further measured H₂O₂ production in the retina and HMC3 cells. As illustrated in Fig. 4F, ICA decreased the H₂O₂ production compared with EAU treatment. Consistently, ICA-elicited enhanced H₂O₂ clearance was found in HMC3 cells (Fig. 4F).

3.5. ICA regulated the GPX4/SLC7A11/ACSL4 pathways

The binding of ICA to PRDX3 prompted us to examine the PRDX3-related signalling pathways regulated by ICA. To investigate the proteins that interact with PRDX3, we constructed biological interaction networks for PRDX3 to identify the top 20 connections using STRING system with "Homo sapiens" and a "high-confidence" setting (Fig. 5A). Among them, glutathione peroxidase 4 (GPX4) is the main enzyme involved in glutathione metabolism and diminishing phospholipid hydroperoxides within a cellular environment [24], which is consistent with the results of the KEGG analysis of ICA-binding proteins, as shown in Fig. 3G. Thus, we focused on the GPX4 signalling pathway. As shown in Fig. 5B and D, the EAU group exhibited lower levels of GPX4 and solute carrier family 7 member 11 (SLC7A11), and higher levels of acyl-CoA synthetase long chain family member 4 (ACSL4). ICA (10 mg/kg) increased GPX4 and SLC7A11 expression and decreased ACSL4 expression (Fig. 5B and D). Furthermore, LPS + IFN- γ addition markedly decreased the mRNA and protein levels of GPX4 and SLC7A11, but

increased the mRNA and protein levels of ACSL4, which were greatly reversed by ICA (10 μ M) treatment (Fig. 5C and E).

3.6. PRDX3 knockdown reversed ICA-elicited retinal microglia M1/M2 phenotypic polarization in vivo

To determine whether ICA elicited retinal microglial M1/M2 phenotypic polarization by increasing PRDX3, we transfected HMC3 cells with PRDX3-shRNA and Vehicle-shRNA, and transfection efficiency was assessed by fluorescence microscope, qPCR and Western blotting (Fig. 6A). Transfected cells were received LPS + IFN- γ + ICA (10 μ M) administration. Then, cells and supernatant were collected to measure M1 and M2 phenotypic polarization after 24 h. Next, we measured the protein expression of M1/M2 markers in the HMC3 cells from both the Vehicle + LPS + IFN- γ + ICA group and the shPRDX3 + LPS + IFN- γ + ICA group. As shown in Fig. 6B and C, ICA-elicited decreased M1 phenotypic polarization and increased M2 phenotypic polarization was no longer detected after blocking PRDX3, which differs from the results shown in Fig. 2 (Fig. 6B and C). Similarly, we also determined the protein levels of the GPX4/SLC7A11/ACSL4 pathways. As indicated in Fig. 6D, the effects of ICA on GPX4/SLC7A11/ACSL4 pathways were reversed by inhibiting PRDX3 compared with Fig. 5 (Fig. 6D). Consistently, the ICA-induced decrease in H₂O₂ production was attenuated in shPRDX3 cells compared with vehicle cells (Fig. 6E). These data implied that ICA could promote microglial M1/M2 phenotypic polarization in a PRDX3-dependent manner.

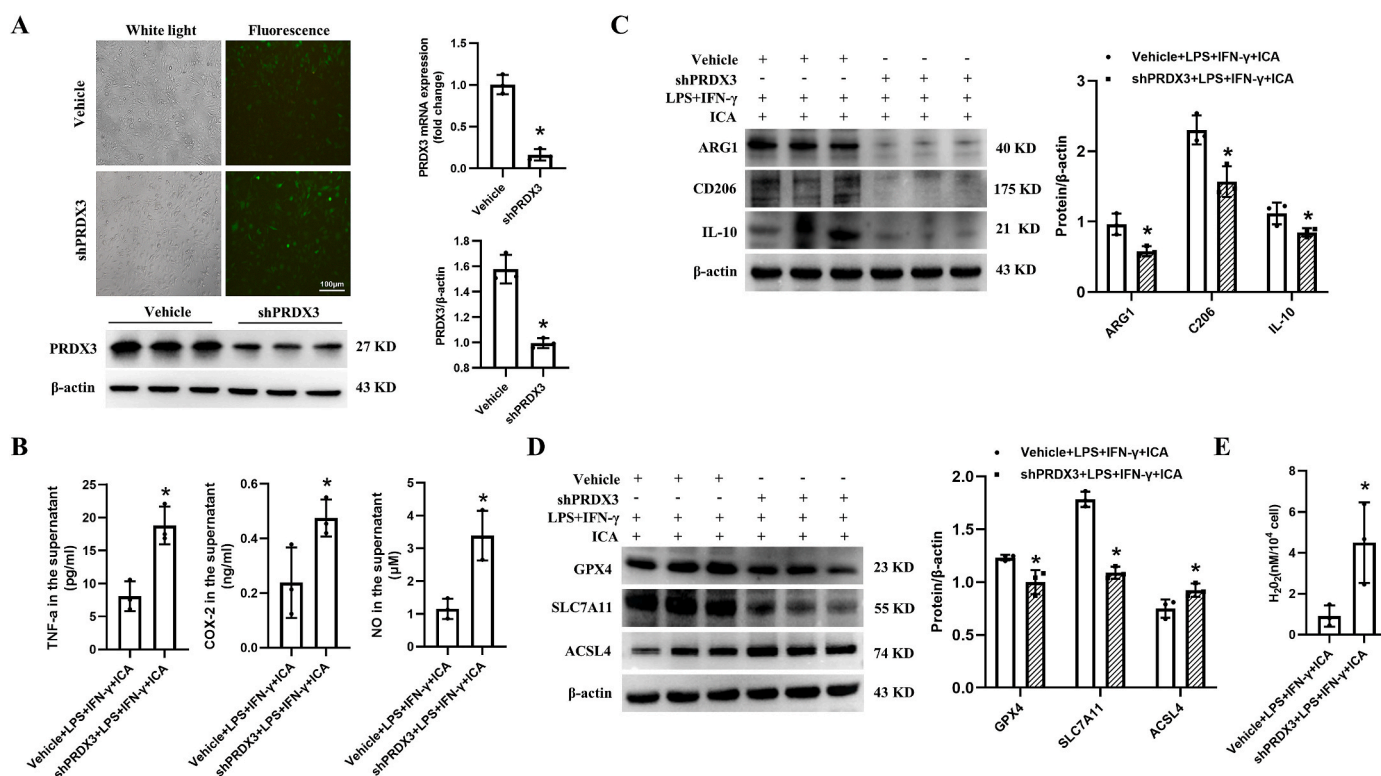


Fig. 6. PRDX3 knockdown reversed ICA-elicited retinal microglial M1/M2 phenotypic polarization in vivo (A) HMC3 cells were exposed to PRDX3-shRNA and Vehicle-shRNA, transfection efficiency was assessed by fluorescence microscope, qPCR and Western blotting. (B) Microglial M1 markers (TNF- α , COX-2, NO) expression of Vehicle + LPS + IFN- γ + ICA (10 μ M) and shPRDX3 + LPS + IFN- γ + ICA (10 μ M) groups as measured by ELISA. (C) M2 markers (ARG1, CD206, IL-10) expression of Vehicle + LPS + IFN- γ + ICA (10 μ M) and shPRDX3 + LPS + IFN- γ + ICA (10 μ M) groups were revealed by Western blotting. (D) Microglial GPX4, SLC7A11 and ACSL4 expression was measured by Western blotting. (E) Microglial H₂O₂ levels were measured. * p < 0.05 compared with the Vehicle + LPS + IFN- γ + ICA (10 μ M) group. (n = 3).

3.7. PRDX3 knockdown aggravated EAU progression and eliminated ICA-elicited microglial M1/M2 phenotypic polarization in vivo

We considered whether ICA exerts protective effects on intraocular inflammation by medicating PRDX3. Therefore, normal mice received intravitreal injections of PRDX3-shRNA (1 μ L) or Vehicle-shRNA (1 μ L) using a microglass syringe for 7 days, and the knockdown efficiency of PRDX3 were evaluated by qPCR and Western blotting (Fig. 7A). Next, on the 7th day after EAU mice immunization, Vehicle + EAU + ICA group received intravitreal injections of Vehicle-shRNA and shPRDX3 + EAU + ICA group received intravitreal injections of PRDX3-shRNA. Then, the two groups received intragastric administration of ICA (10 mg/kg) once a day for 7 consecutive days. As shown in Fig. 7B, both conjunctival and ciliary hyperaemia and infiltration of anterior chamber inflammatory cells were aggravated by shPRDX3. Moreover, the pathological view displayed more retinal folds and inflammatory cells in the shPRDX3 + EAU + ICA group. The clinical score and pathological score were consistent with the above findings (Fig. 7B). Furthermore, the integrity of BRB and quantification of occludin protein showed a significant decrease in the shPRDX3 + EAU + ICA group (Fig. 7C). Next, we measured the retinal protein expression of M1/M2 markers. As shown in Fig. 7D, the ICA-elicited reduced M1 phenotypic polarization and increased M2 phenotypic polarization was no longer detected after blocking PRDX3 compared with those in Fig. 2 (Fig. 7D). Similarly, the effects of ICA on GPX4/SLC7A11/ACSL4 pathways and decreasing H₂O₂ production were reversed by inhibiting PRDX3 which contrasted with the results shown in Fig. 5 (Fig. 7E). Consistently, ICA-mediated decrease in H₂O₂ activity eliminated after inhibiting PRDX3 (Fig. 7F). These results not only confirm the indispensable PRDX3 during ICA-elicited anti-uveitis properties, but

also indicate that PRDX3 plays a vital role in the switching cycle from M1 microglia to M2 microglia.

4. Discussion

Through our experiments, we have provided strong evidence indicating that ICA could alleviate EAU pathogenesis. This finding further led to the novel discovery that ICA could modulate microglial M1/M2 phenotypic polarization in vivo and in vitro. We further devised a strategy to investigate ICA-binding proteins worldwide by integrating biotinylated ICA with a human proteome microarray. In this way, we provided evidence that ICA acted on PRDX3, subsequently activating the GPX4/SLC7A11/ACSL4 pathways and decreasing H₂O₂ production. As expected, ICA-shifted microglial M1/M2 phenotypic polarization was eliminated in PRDX3-deficient HMC3 cells in vitro. In parallel, we also found that the depletion of PRDX3 in retina not only exacerbated intraocular inflammation but also blocked the effects of modulating microglial M1/M2 phenotypic polarization in vivo. In view of the abovementioned well-documented evidence, ICA might be a potential therapeutic treatment for uveitis.

Our findings indicated that ICA could alleviate EAU pathogenesis. Notably, ICA could also modulate microglial M1/M2 phenotypic polarization in vivo and in vitro. Under different forms of stimulation involving LPS and IRBP, microglia become polarized towards the M1 phenotype accompanied by overexpression of TNF- α , COX-2 and NO/iNOS. Mounting evidence has demonstrated that accumulated inflammatory factors can result in retinal degeneration/damage and blindness [25,26]. Fortunately, we also found that ICA treatment polarized microglia from the M1 phenotype to the M2 phenotype, accompanied by

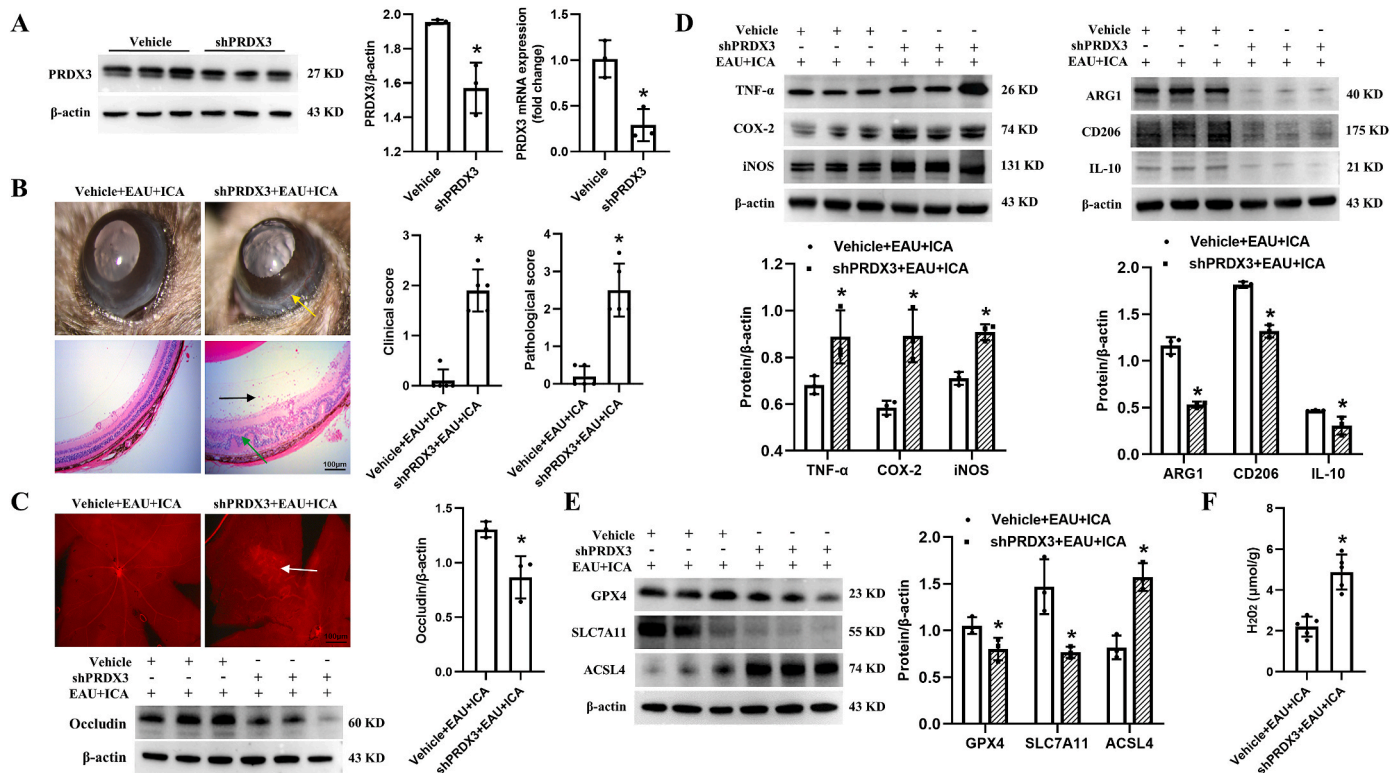


Fig. 7. PRDX3 knockdown aggravated EAU progression and eliminated ICA-elicited microglial M1/M2 phenotypic polarization in vivo (A) Retinal PRDX3 knockdown efficiency were detected by qPCR and Western blotting. (B) Anterior chamber inflammation and retinal histopathological staining of Vehicle + EAU + ICA and shPRDX3 + EAU + ICA groups. Clinical scores and pathology scores were also shown. (scale bar, 100 μ m; yellow arrow, conjunctival and/or ciliary congestion; black arrow, infiltration of inflammatory cells; green arrow, retinal folds). (C) Retinal integrity and retinal occludin protein quantification (scale bar, 100 μ m; white arrow, retinal vascular leakage). (D) The protein expression of retinal M1 markers (TNF- α , COX-2, iNOS) and M2 markers (ARG1, CD206, IL-10) were detected by Western blotting. (E) The protein expression of retinal GPX4, SLC7A11 and ACSL4 were detected by Western blotting. (F) Retinal H₂O₂ level were measured. * p < 0.05 compared with the Vehicle + EAU + ICA group. (n = 3–5).

overexpression of ARG1, CD206 and IL-10, which subsequently protected the retina. CD206 can be linked to apoptotic and necrotic cells, promoting the elimination of dying cells and preventing secondary damage [27]. In the injured mice spinal cord, both ARG1 and CD206 promoted axonal growth [28]. In addition, subretinal injection of rAAV-2 encoding murine IL-10 into the retina of C57BL/6 mice significantly decreases EAU severity [29]. Collectively, these data emphasize that ICA-elicited microglial M1/M2 polarization might be involved in the improvement of EAU progression.

The identification of drug-binding proteins is one of the effective ways to elucidate the mechanisms of drug targets. We utilized HuProt microarrays for the first time for ICA-binding proteins, and 246 candidate ICA-interacting proteins were identified. When the proteins were sorted in descending order by their IMean ratio, the top interacting protein was ALDH9A1 (IMean ratio of 2.301), the second highest-ranking interacting protein was PRDX3 (IMean ratio of 2.095). However, when we detected the protein expression of ALDH9A1 and PRDX3 in EAU retina after ICA application, we did not observe significant difference in ALDH9A1 in ICA-treated EAU mice (Fig. S1). Interestingly, ICA increased the protein expression of PRDX3. We assume that, at least in this EAU system, ICA-elicited action through ALDH9A1 interaction does not occur. Thus, we identified PRDX3 as a potential target of ICA. This interaction was further validated by molecular docking, which showed that ICA may bind to PRDX3 in the pocket between the two chains. Notably, Lys135 and Glu162 on chain A and Thr44 on chain B, thus sites might represent key regulatory points of the biological function of PRDX3. Further studies are needed to perform to verify the bind sites between PRDX3 and ICA.

Additional questions have also emerged: which downstream signaling pathway is triggered by PRDX3? Biological interaction networks for PRDX3 were constructed automatically by the STRING system with the settings “*Homo sapiens*”, “20 connections” and “high-confidence”. We further constructed GPX4/SLC7A11/ACSL4 pathways. A previous study indicated that GPX4 is the main enzyme involved in glutathione metabolism, which is required for the maturation of photoreceptor cells [30]. GSH protects against oxidative damage in RPE cells [31]. SLC7A11, a key component of cystine/glutamate transporter, regulates the level of cellular lipid peroxidation. SLC7A11 reduces laser-induced choroidal neovascularization by inhibiting RPE ferroptosis and VEGF production. Since decreased PRDX3 and disruptive redox homeostasis are peculiar signs of EAU, ICA targeted on PRDX3 to upregulate GPX4 and SLC7A11, decrease ACSL4 expression, and restore normal levels of H₂O₂ simultaneously. This regulation further maintained redox homeostasis and amplified antioxidative effects. Therefore, we anticipate that ICA represents a promising strategy for autoimmune uveitis therapy.

Collectively, we investigated the potential binding proteins of ICA, which will provide a valuable resource for ICA-binding proteins. Furthermore, we verified PRDX3 as a key target, and this targeting could modulate microglial M1/M2 phenotypic polarization and alleviate EAU. However, its clinical application requires further research.

Author contributions

G.W and X.L performed this experiment; S.H designed this study; N.L and X.W and S.H participated in reagents or tools; W.L, W.F, R.L and J.L analysed all data, G.W and X.L wrote the paper.

Declaration of interests

The authors declare the following financial interests/personal relationships which may be considered as potential competing interests: None.

Acknowledgements

This work was supported by National Natural Science Foundation

Project of China (81873678, 82070951), the Innovative Research Group Project of Chongqing Education Commission (CXQT19015), the Chongqing Natural Science Foundation (cstc2019jcyj-msxmX0120), the innovation supporting Plan of Overseas Study of Chongqing (cx2018010), National Key Clinical Specialties Construction Program of China, Chongqing Key Laboratory of Ophthalmology (CSTC, 2008CA5003), Natural Science Foundation Project of Chongqing Medical University (W0047).

Appendix A. Supplementary data

Supplementary data to this article can be found online at <https://doi.org/10.1016/j.redox.2022.102297>.

References

- [1] M. Feng, S.P. Zhou, T. Liu, et al., Association between interleukin 35 gene single nucleotide polymorphisms and the uveitis immune status in a Chinese Han population, *Front. Immunol.* 12 (2021) 758554.
- [2] M. Kasper, M. Heming, D. Schafflick, et al., Intraocular dendritic cells characterize HLA-B27-associated acute anterior uveitis, *Elife* 10 (2021).
- [3] Y.H. Chen, M. Eskandarpour, X. Zhang, et al., Small-molecule antagonist of VLA-4 (GW559090) attenuated neuro-inflammation by targeting Th17 cell trafficking across the blood-retinal barrier in experimental autoimmune uveitis, *J. Neuroinflammation* 18 (2021) 49.
- [4] J. Hu, C. Wang, X. Huang, et al., Gut microbiota-mediated secondary bile acids regulate dendritic cells to attenuate autoimmune uveitis through TGR5 signaling, *Cell Rep.* 36 (2021) 109726.
- [5] S.J. Chen, T.B. Lin, H.Y. Peng, et al., Protective effects of Fucoxanthin Dampen pathogen-associated molecular pattern (PAMP) lipopolysaccharide-induced inflammatory action and elevated intraocular pressure by activating Nrf2 signaling and generating reactive oxygen species, *Antioxidants* 10 (2021).
- [6] G. Emmi, A. Bettiol, E. Niccolai, et al., Butyrate-rich diets improve redox status and Fibrin lysis in Behçet's syndrome, *Circ. Res.* 128 (2021) 278–280.
- [7] J.B. Goodman, F. Qin, R.J. Morgan, et al., Redox-resistant SERCA [Sarco(endo) plasmic reticulum calcium ATPase] attenuates oxidant-stimulated mitochondrial calcium and apoptosis in cardiac myocytes and pressure overload-induced myocardial failure in mice, *Circulation* 142 (2020) 2459–2469.
- [8] H. Huang, S. Zhang, Y. Li, et al., Suppression of mitochondrial ROS by prohibitin drives glioblastoma progression and therapeutic resistance, *Nat. Commun.* 12 (2021) 3720.
- [9] S. Elumalai, U. Karunakaran, J.S. Moon, et al., High glucose-induced PRDX3 acetylation contributes to glucotoxicity in pancreatic β -cells: prevention by Teneligliptin, *Free Radic. Biol. Med.* 160 (2020) 618–629.
- [10] A.P. Rebelo, I. Eidhof, V.P. Cintra, et al., Biallelic loss-of-function variations in PRDX3 cause cerebellar ataxia, *Brain* 144 (2021) 1467–1481.
- [11] Z. Wang, R. Sun, G. Wang, et al., SIRT3-mediated deacetylation of PRDX3 alleviates mitochondrial oxidative damage and apoptosis induced by intestinal ischemia/reperfusion injury, *Redox Biol.* 28 (2020) 101343.
- [12] Y. Okunuki, R. Mukai, T. Nakao, et al., Retinal microglia initiate neuroinflammation in ocular autoimmunity, *Proc. Natl. Acad. Sci. U.S.A.* 116 (2019) 9989–9998.
- [13] Y. Shen, R. Yang, J. Zhao, et al., The histone deacetylase inhibitor belinostat ameliorates experimental autoimmune encephalomyelitis in mice by inhibiting TLR2/MyD88 and HDAC3/NF- κ B p65-mediated neuroinflammation, *Pharmacol. Res.* 176 (2022) 105969.
- [14] X. Han, X. Chen, S. Chen, et al., Tetramethylpyrazine attenuates endotoxin-induced retinal inflammation by inhibiting microglial activation via the TLR4/NF- κ B signalling pathway, *Biomed. Pharmacother* 128 (2020) 110273.
- [15] Z. Cheng, Y. Yang, F. Duan, et al., Inhibition of Notch 1 signaling alleviates endotoxin-induced inflammation through modulating retinal microglia polarization, *Front. Immunol.* 10 (2019) 389.
- [16] Y. Huang, J. He, H. Liang, et al., Aryl hydrocarbon receptor regulates apoptosis and inflammation in a murine model of experimental autoimmune uveitis, *Front. Immunol.* 9 (2018) 1713.
- [17] S. Liu, D.S. Xu, M. Li, et al., Icarin attenuates endothelial-mesenchymal transition via H19/miR-148b-3p/ELF5 in ox-LDL-stimulated HUVECs, *Mol. Ther. Nucleic Acids* 23 (2021) 464–475.
- [18] X. Li, I. Khan, W. Xia, et al., Icarin enhances youth-like features by attenuating the declined gut microbiota in the aged mice, *Pharmacol. Res.* 168 (2021) 105587.
- [19] B. Zhang, G. Wang, J. He, et al., Icarin attenuates neuroinflammation and exerts dopamine neuroprotection via an Nrf2-dependent manner, *J. Neuroinflammation* 16 (2019) 92.
- [20] W.F. Chen, L. Wu, Z.R. Du, et al., Neuroprotective properties of icaridin in MPTP-induced mouse model of Parkinson's disease: involvement of PI3K/Akt and MEK/ERK signaling pathways, *Phytomedicine* 25 (2017) 93–99.
- [21] E.C. Mbanefo, M. Yan, M. Kang, et al., STAT3-Specific single domain nanobody inhibits expansion of pathogenic Th17 responses and suppresses uveitis in mice, *Front. Immunol.* 12 (2021) 724609.

- [22] H.N. Zhang, L. Yang, J.Y. Ling, et al., Systematic identification of arsenic-binding proteins reveals that hexokinase-2 is inhibited by arsenic, *Proc. Natl. Acad. Sci. U. S.A.* 112 (2015) 15084–15089.
- [23] J.W. Wyatt, D.A. Korasick, I.A. Qureshi, et al., Inhibition, crystal structures, and in-solution oligomeric structure of aldehyde dehydrogenase 9A1, *Arch. Biochem. Biophys.* 691 (2020) 108477.
- [24] H. Liu, F. Forouhar, T. Seibt, et al., Characterization of a patient-derived variant of GPX4 for precision therapy, *Nat. Chem. Biol.* 18 (2022) 91–100.
- [25] Y. Tu, L. Li, L. Zhu, et al., Geniposide attenuates hyperglycemia-induced oxidative stress and inflammation by activating the Nrf2 signaling pathway in experimental diabetic retinopathy, *Oxid. Med. Cell. Longev.* 2021 (2021) 9247947.
- [26] A.W. Qiu, D.R. Huang, B. Li, et al., IL-17A injury to retinal ganglion cells is mediated by retinal Müller cells in diabetic retinopathy, *Cell Death Dis.* 12 (2021) 1057.
- [27] J.M. Jaynes, R. Sable, M. Ronzetti, et al., Mannose receptor (CD206) activation in tumor-associated macrophages enhances adaptive and innate antitumor immune responses, *Sci. Transl. Med.* 12 (2020).
- [28] A. Kisucka, K. Bimbova, M. Bacova, et al., Activation of neuroprotective microglia and astrocytes at the lesion site and in the adjacent segments is crucial for spontaneous locomotor recovery after spinal cord injury, *Cells* 10 (2021).
- [29] C.A. Broderick, A.J. Smith, K.S. Balaggan, et al., Local administration of an adeno-associated viral vector expressing IL-10 reduces monocyte infiltration and subsequent photoreceptor damage during experimental autoimmune uveitis, *Mol. Ther.* 13 (2006) 829.
- [30] T. Ueta, T. Inoue, T. Furukawa, et al., Glutathione peroxidase 4 is required for maturation of photoreceptor cells, *J. Biol. Chem.* 287 (2012) 7675–7682.
- [31] Y. Sun, Y. Zheng, C. Wang, et al., Glutathione depletion induces ferroptosis, autophagy, and premature cell senescence in retinal pigment epithelial cells, *Cell Death Dis.* 9 (2018) 753.